CFD Analysis of the ONERA M6 Wing

Numerical Investigation of Transonic Flow

AUTHOR
WACOMBER Romain

DATE
August 2026

Contents

List of Figures

1 Introduction

The ONERA M6 wing is a well-known benchmark geometry widely used for the validation of Computational Fluid Dynamics (CFD) methods in transonic aerodynamic flows [1]. Developed and experimentally tested by ONERA (the French Aerospace Laboratory), the wing has a swept, tapered geometry and was designed to generate complex transonic flow phenomena, including shock waves and shock-induced flow separation. Extensive wind-tunnel measurements are available for several operating conditions, providing detailed pressure distributions over the wing surface. These experimental data make the ONERA M6 wing particularly suitable for assessing the accuracy of numerical methods, turbulence models, and spatial discretization schemes. For this reason, the ONERA M6 case remains a standard reference for studying three-dimensional compressible flow and evaluating the ability of CFD simulations to accurately predict shock-wave position and aerodynamic performance.

Two different test cases are available for the ONERA M6 wing. The case studied in this work is test case 2308, for which the boundary conditions are described in the following section.

The objective of this study is to perform several CFD simulations using two turbulence models : Spalart-Allmaras and $k - \omega\ SST$ and to compare the numerical results with the available experimental data. All the CFD simulations are realized with OpenFOAM v2412.

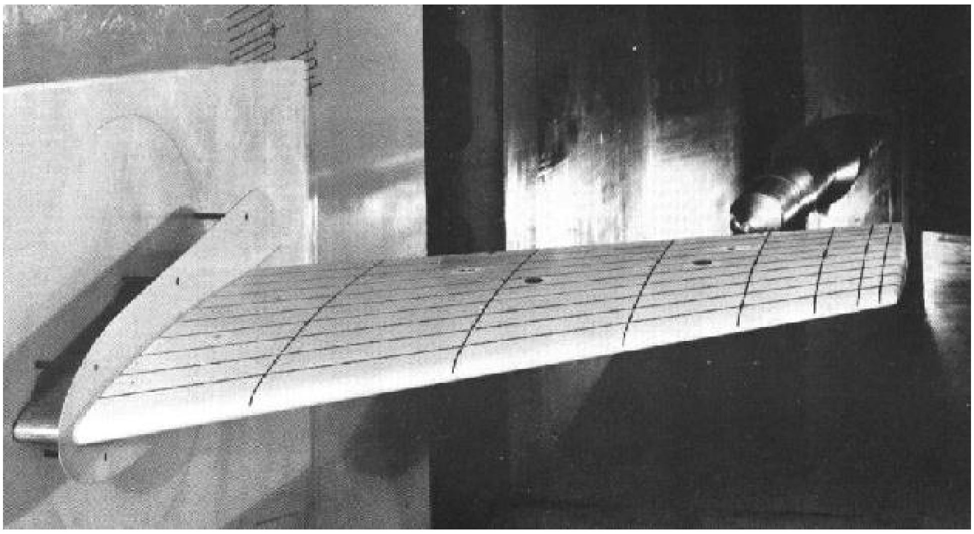

Figure 1: Onera M6 wing used for experimental test

2 Flow conditions

As explained above, the ONERA M6 wing was designed to perform transonic flow ($M_\infty > 0.8$). The test case 2308 consist of air at the condition described in Table 1.

M_∞	Re_c	AOA [deg]	T_∞ [K]	P_∞ [Pa]
0.84	14.6×10^6	3.06	300	98154

Table 1: Flow conditions

The air with $M = 28.9\ kg.kmol^{-1}$ is considered as a perfect gas, then density ρ is calculated using equation 1.

$$\rho = \frac{PM}{RT} \tag{1}$$

The specific heat capacity at constant pressure C_p is considered constant and equal to $1005\ J.kg^{-1}.K^{-1}$.

The dynamic viscosity μ and thermal conductivity κ are calculated using Sutherland law, reminded in equation 2 and 3.

$$\mu = A_s \frac{\sqrt{T}}{1 + \frac{T_s}{T}} \tag{2}$$

$$\kappa = \mu(c_p - R)\left(1.32 + 1.77\frac{R}{c_p - R}\right) \tag{3}$$

With $A_s = 1.4792 \times 10^6$; $T_s = 116\ K$ and $R = 287\ J.kg^{-1}.K^{-1}$

For the simulations performed with the Spalart–Allmaras turbulence model, the modified turbulent kinematic viscosity $\tilde{\nu}$ must be specified at each boundary. At the freestream boundary, the condition

$$\tilde{\nu} = 3\nu_\infty = 4.855 \times 10^{-5}\ \mathrm{m^2\,s^{-1}}$$

is imposed. At the wing surface, a zero value is prescribed:

$$\tilde{\nu} = 0\ \mathrm{m^2\,s^{-1}}$$

For simulations using the k–ω SST turbulence model, boundary conditions must be specified for both the turbulent kinetic energy k and the specific dissipation rate ω. At the freestream boundary, the turbulent kinetic energy is defined as

$$k = \frac{3}{2}(IU_\infty)^2$$

where I denotes the turbulence intensity, which is set to 0.2%. This results in a freestream value of

$$k = 0.51\ \mathrm{m^2\,s^{-2}}$$

At the wing surface, the `kqRWallFunction` wall boundary condition is applied.

The freestream value of ω is determined from

$$\omega = \frac{\sqrt{k}}{C_\mu^{1/4} L}$$

where $C_\mu = 0.09$ and L is a characteristic turbulent length scale, here taken as the mean aerodynamic chord of the wing. This gives a freestream value of

$$\omega = 2\ \mathrm{s^{-1}}$$

At the wing surface, the `omegaWallFunction` boundary condition is used.

3 Meshing

For each turbulence model, the same three meshes are used. A reference mesh containing 2,163,546 cells was generated, while the other two meshes were obtained by coarsening and refining the reference mesh using a refinement factor of $r = 1.337$. This results in 889,600 cells for the coarse mesh and 5,089,395 cells for the fine mesh, respectively.

To accurately model the boundary layer, prism layers are generated near the wing surface for each mesh in order to ensure that $30 < y^+ < 300$. Figure 4 shows the distribution of y^+ values over the wing surface for the reference mesh using the Spalart–Allmaras turbulence model. A similar y^+ distribution is obtained for the other meshes and turbulence models, with the large majority of the wing surface remaining within the target range $30 < y^+ < 300$. All meshes are generated using the open-source meshing tool *snappyHexMesh*.

The computational domain is bounded by a hemisphere whose dimensions are considered sufficiently large to minimize the influence of the far-field boundaries on the flow around the wing.

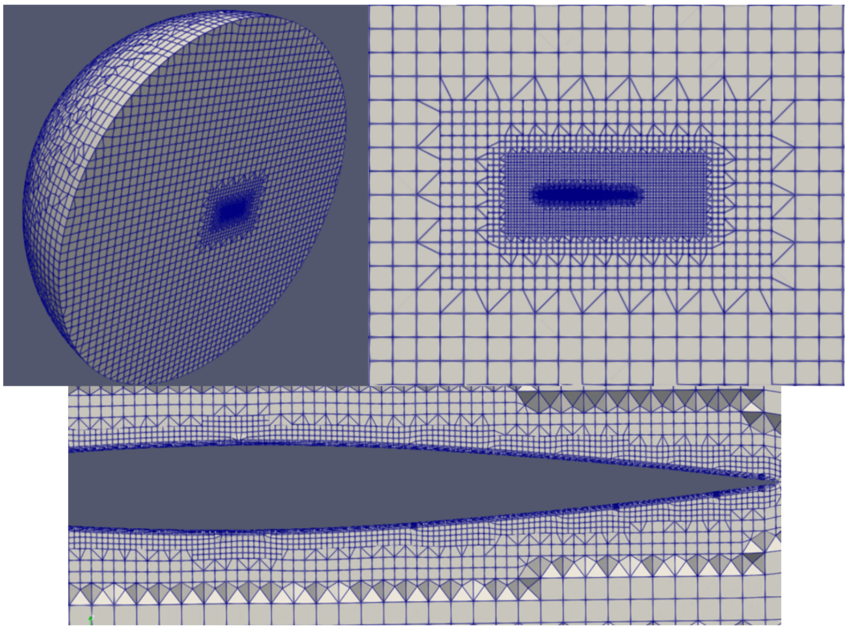

Figure 2: Volume Mesh of the reference mesh

4 Interpolation Schemes and Solutions Algorithm

In order to solve the governing equations, appropriate gradient and divergence discretization schemes must be specified. For all simulations, the gradients are discretized using the second-order Gauss linear scheme. To improve numerical stability, a limiter is applied to the velocity gradient as well as to the gradients of the turbulence variables k and ω when using the k-ω SST model.

For the divergence terms, the same discretization scheme is used for the momentum, energy, and turbulence equations. The selected scheme is Gauss linearUpwind, which is a second-order, unbounded, upwind-biased discretization scheme. It reconstructs the face values using the upwind cell value together with an explicit gradient-based correction,

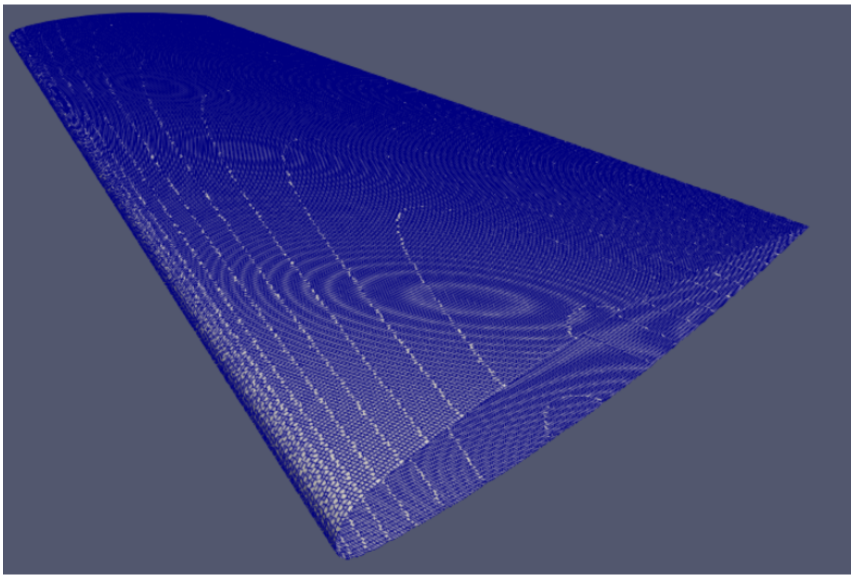

Figure 3: Surface Mesh of the reference mesh

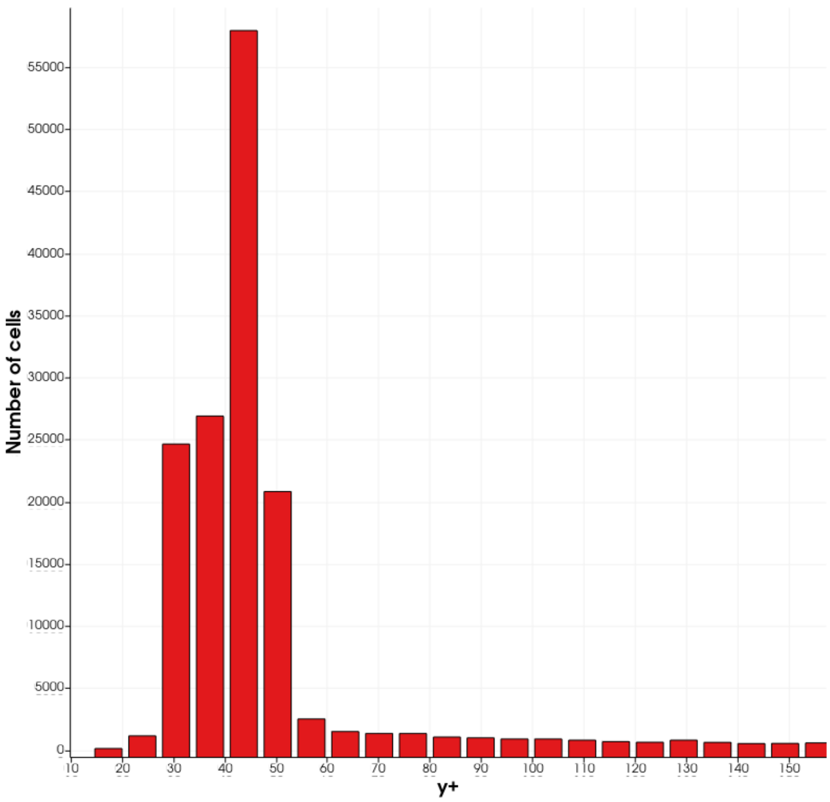

Figure 4: y^+ distribution for the reference mesh using the Spalart-Allmaras turbulence model

providing higher spatial accuracy than the first-order upwind scheme while retaining an upwind-biased formulation. This approach reduces numerical diffusion and improves the resolution of flow gradients, which is particularly important for accurately capturing the aerodynamic features of transonic flows, including shock waves.

For each discretized equation, the GAMG (Geometric-Algebraic MultiGrid) solver is used in combination with a Gauss-Seidel smoother. Finally, the pressure-velocity coupling is handled using the SIMPLEC algorithm (Semi-Implicit Method for Pressure-Linked Equations Consistent).

5 Results

This section presents the results obtained with the Spalart–Allmaras and k–ω SST turbulence models. First, the lift and drag coefficients obtained with the three meshes are compared, and a mesh-independence study is performed using the Grid Convergence Index (GCI) method. The pressure coefficient distributions are then analysed at several spanwise stations and over the entire wing surface.

5.1 Lift and Drag Coefficients

The lift and drag coefficients obtained with the Spalart–Allmaras and k–ω SST turbulence models are summarised in Table 2.

Grid	h [m]	C_L (Spalart–Allmaras)	C_D (Spalart–Allmaras)	C_L (k–ω SST)	C_D (k–ω SST)
Coarse	0.1330	0.2198	0.01988	0.2178	0.01946
Mid	0.0990	0.2430	0.01798	0.2437	0.01794
Fine	0.0744	0.2504	0.01743	0.2533	0.01754
Extrapolation	0	0.2540	0.01721	0.2589	0.01740

Table 2: Lift and drag coefficients obtained for the three meshes and the Richardson-extrapolated values.

The values reported in Table 2 for $h = 0$ correspond to Richardson extrapolations toward a theoretically infinitely fine mesh. The extrapolated values are calculated using the two finest meshes, while the observed order of convergence is determined from the three mesh levels.

Assuming an approximately constant refinement ratio $r = 1.337$, the observed order of convergence is calculated as

$$\tilde{p} = \frac{\ln\left|\dfrac{\phi_3 - \phi_2}{\phi_2 - \phi_1}\right|}{\ln(r)} \tag{4}$$

where ϕ_1, ϕ_2, and ϕ_3 denote the values obtained with the fine, medium, and coarse meshes, respectively.

The observed orders of convergence are $\tilde{p}_{C_L} = 3.88$ and $\tilde{p}_{C_D} = 4.27$ for the Spalart–Allmaras model and $\tilde{p}_{C_L} = 3.42$ and $\tilde{p}_{C_D} = 4.61$ for the k–ω SST model.

The asymptotic convergence ratios obtained for the four quantities are 1.03 and 0.97 for C_L and C_D, respectively, with the Spalart–Allmaras model, and 1.04 and 0.98 with the k–ω SST model. Since these values are close to the theoretical value of unity,

$$\frac{GCI_{23}}{r^{\tilde{p}}GCI_{12}} \approx 1$$

the three-grid sequences can be considered to lie within the asymptotic range of convergence. Consequently, the Richardson-extrapolated values and the corresponding GCI estimates provide consistent estimates of the spatial discretization error.

Figure 5 shows the evolution of the lift and drag coefficients with mesh refinement for both turbulence models. In both cases, the aerodynamic coefficients progressively approach their extrapolated values as the mesh is refined.

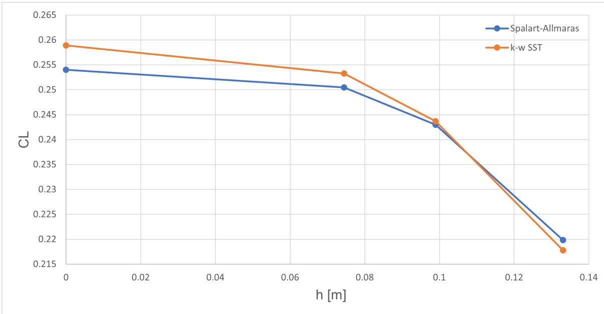

(a)

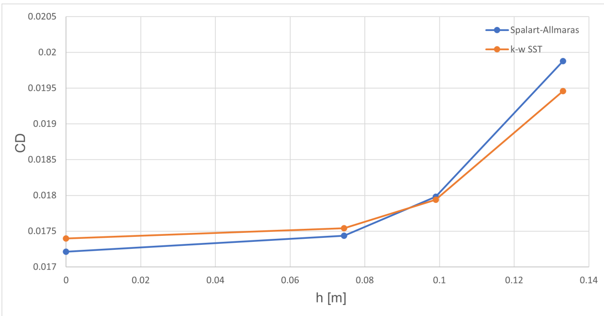

(b)

Figure 5: Mesh-convergence study for the lift coefficient (a) and drag coefficient (b).

5.2 Pressure Distribution

The pressure coefficient distributions obtained with both turbulence models and the three mesh levels are presented in the following figures. The distributions are evaluated at seven spanwise stations: $\eta = 0.20$, 0.44, 0.65, 0.80, 0.90, 0.96, and 0.99. Experimental pressure coefficient data are also available at these locations, allowing a direct comparison between the numerical results and the experimental measurements.

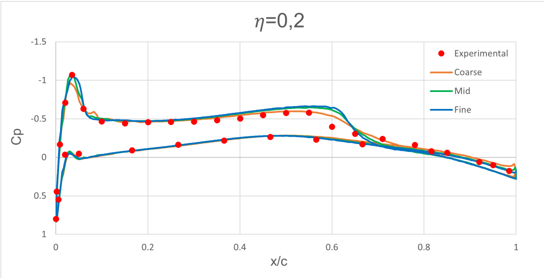

(a)

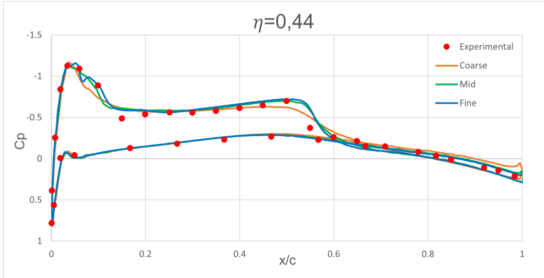

(b)

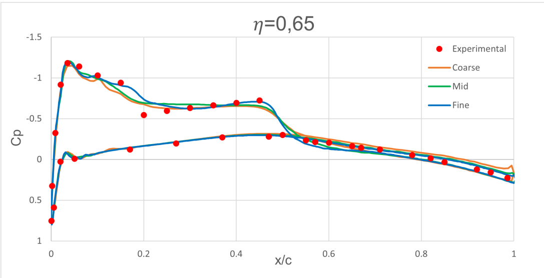

(c)

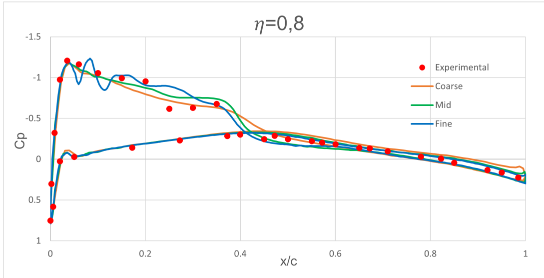

(d)

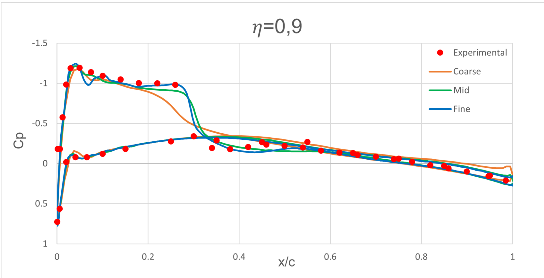

(e)

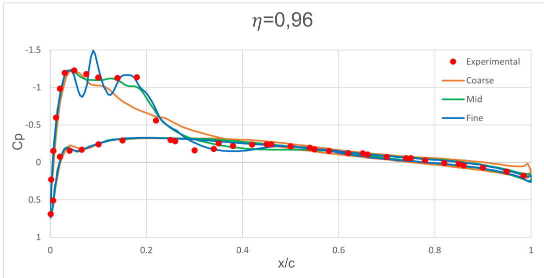

(f)

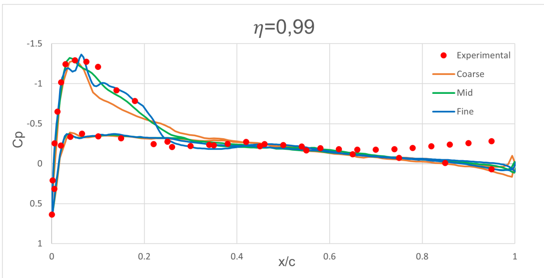

(g)

Figure 6: Pressure coefficient distributions at different spanwise stations obtained with the Spalart–Allmaras turbulence model.

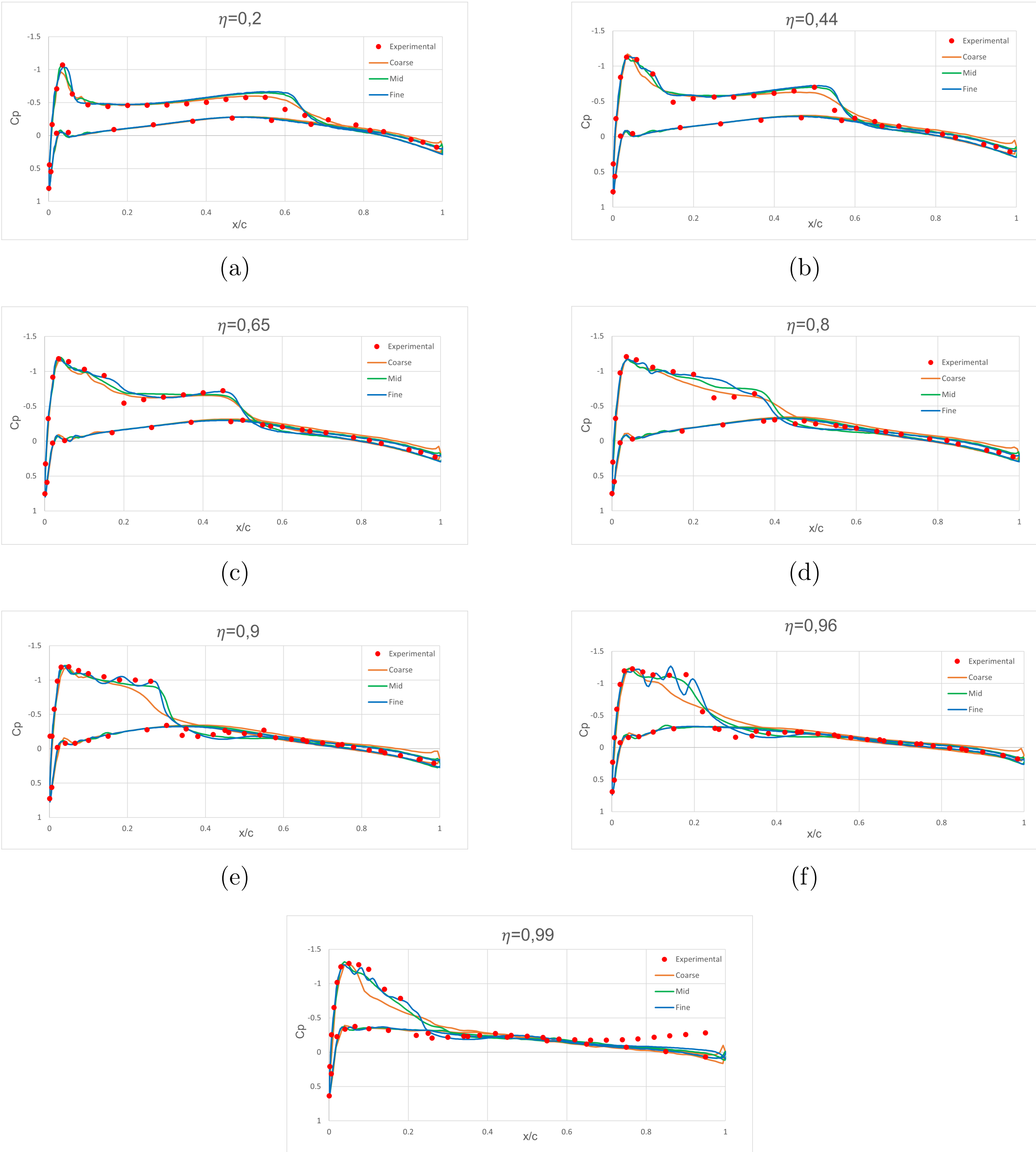

(g)

Figure 7: Pressure coefficient distributions at different spanwise stations obtained with the k–ω SST turbulence model.

Figures 6 and 7 show an overall good agreement between the numerical results and the experimental measurements. Both turbulence models predict very similar pressure distributions over most of the span. Nevertheless, the k–ω SST model provides slightly closer agreement with the experimental data at some spanwise stations : $\eta = 0.8; 0.9; 0.96$

The pressure coefficient distribution over the complete wing surface is shown in Figure 8. Both turbulence models reproduce the characteristic shock-wave structure of the ONERA M6 wing. In particular, the two shock branches form the characteristic lambda-shaped shock pattern over the upper surface of the wing.

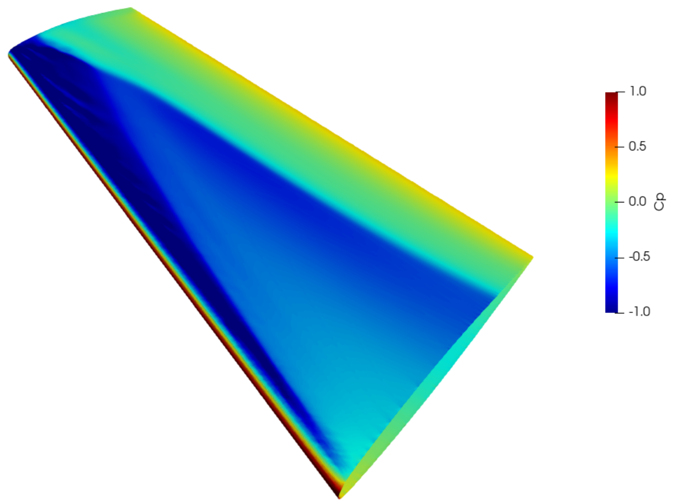

(a)

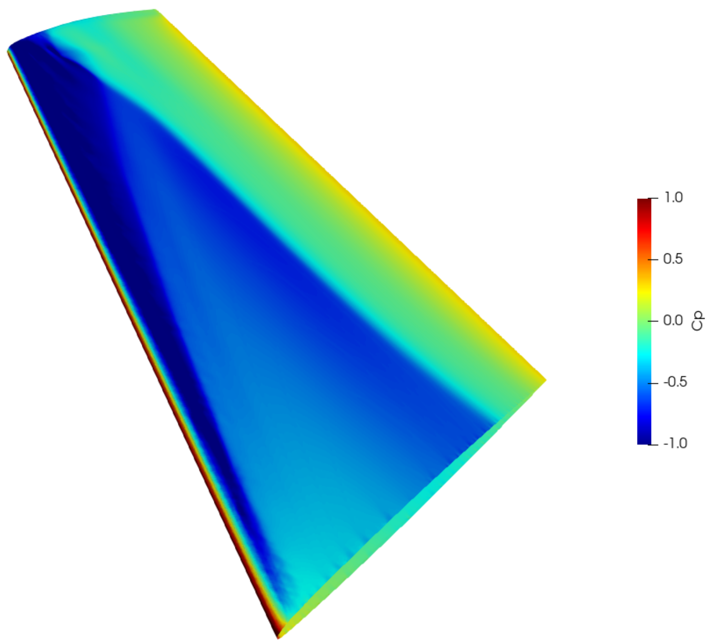

(b)

Figure 8: C_p distribution over the wing surface obtained with the Spalart–Allmaras (a) and k–ω SST (b) turbulence models.

6 Conclusion

The numerical study of the ONERA M6 wing was performed using the Spalart–Allmaras and k–ω SST turbulence models on three different mesh resolutions. The mesh-convergence study showed a consistent convergence of both lift and drag coefficients, with the GCI asymptotic ratios remaining close to unity. The Richardson extrapolation therefore provides a reliable estimate of the aerodynamic coefficients for an infinitely refined mesh.

The pressure coefficient distributions obtained with both turbulence models show good agreement with the experimental data at the different spanwise stations. The k–ω SST model provides slightly better agreement at some sections, particularly in the regions affected by the shock waves. Both turbulence models are also able to reproduce the characteristic lambda-shaped shock structure observed on the upper surface of the ONERA M6 wing.

Overall, the results confirm that the numerical methodology used in this study is able to reproduce the main aerodynamic characteristics of the transonic flow around the ONERA M6 wing.

References

[1] NASA Turbulence Modeling Resource. *3D ONERA M6 Wing Validation Case*. 2021. URL: https://tmbwg.github.io/turbmodels/onerawingnumerics_val.html.